Damage mechanisms in hybrid composites: experimental characterisation and energy-based numerical analysis

João M. Parente
C-MAST, Center for Mechanical and Aerospace Science and Technologies, Universidade da Beira Interior, Rua Marquês d'Avila e Bolama 6201-001 Covilhã, Portugal
joao.miguel.parente@ubi.pt, http://orcid.org/0000-0002-4875-5838

Luis M. Ferreira
Grupo de Elasticidad y Resistencia de Materiales, Escuela Técnica Superior de Ingeniería, Universidad de Sevilla, Camino Descubrimientos, S/N, Sevilla 41092, España
Escuela Superior Politécnica, Universidad de Sevilla, C/ Virgen de África, 7, Sevilla 41011, España
lmarques@us.es, http://orcid.org/0000-0002-5223-5309

Paulo N.B. Reis
University of Coimbra CEMMPRE, ARISE, Department of Mechanical Engineering, 3030-788 Coimbra, Portugal
paulo.reis@dem.uc.pt, http://orcid.org/0000-0001-5203-3670

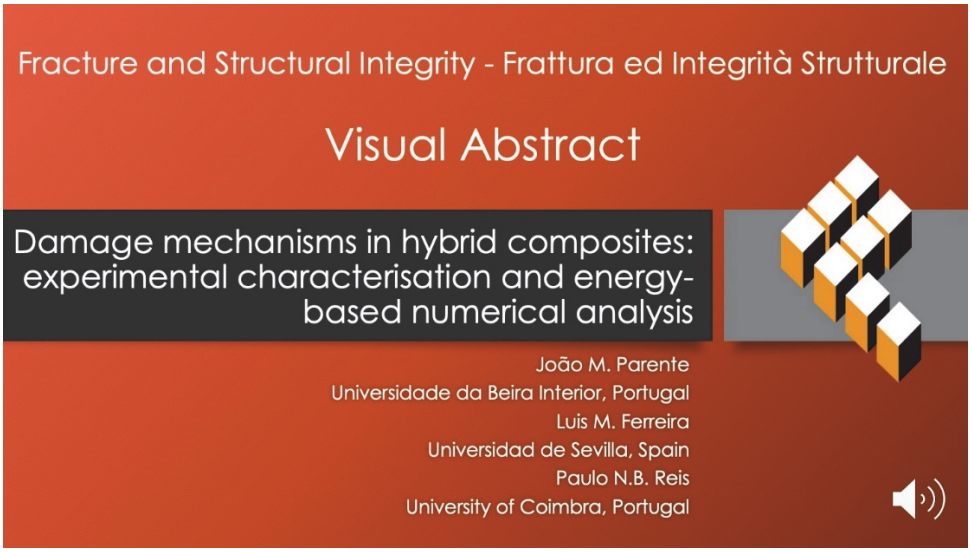

Citation: Parente J.M, Ferreira L.M., Reis, P.N.B., Damage mechanisms in hybrid composites: experimental characterisation and energy-based numerical analysis, Fracture and Structural Integrity, 73 (2025) 139-152.

Received: 06.04.2025
Accepted: 20.05.2025
Published: 21.05.2025
Issue: 07.2025

KEYWORDS. Fiber's hybridisation, Epoxy composites, Damage mechanisms, Bending behaviour; Numerical analysis.

INTRODUCTION

Hybrid fibre-reinforced polymer composites, particularly those combining carbon and glass fibres with an epoxy matrix, have garnered significant interest in recent years due to their exceptional mechanical properties, lightweight nature, and versatility in applications ranging from aerospace to automotive industries. The synergetic effect of carbon fibres, which possess high stiffness and strength, combined with the toughness and relatively low cost of glass fibres, makes these hybrid composites an attractive choice for structural applications subjected to complex loading conditions. However, understanding the failure mechanisms of these materials under bending loads is critical for optimising their design and ensuring reliability in real world applications.

Bending tests are a widely to evaluate the mechanical performance of composite materials because they simulate the bending stresses encountered in service. However, experimental testing alone can be insufficient for fully understanding the phenomena that occur during bending testing as these events often occur in fractions of a second. Numerical methods, such as finite element (FE) analysis, can serve as valuable tools for understanding the material response during bending. Several studies have employed this approach to investigate mechanical behaviours under flexural loading. For instance, Dong et al. [1, 2] used FE models to examine the bending characteristics of hybrid composites incorporating carbon, glass, and flax fibres. Their findings revealed that the combination of carbon and glass fibre enhanced the bending strength of the composite, exceeding predictions based on the rule of mixtures. The study identified an optimal stacking sequence in which carbon/epoxy plies were positioned on the exterior and glass or flax plies were positioned on the interior, enabling material optimisation. Gopalraj et al. [3], for example, employed FE models to evaluate the mechanical properties of recycled carbon fibre and recycled glass fibre reinforced epoxy composites. Their investigation demonstrated that damage initiation in tensile tests primarily occurs due to fibre-matrix interface failure and internal defects. Additionally, the authors found that composites with higher fibre volume fractions exhibited enhanced impact resistance. In another study, Shaikh et al. [4] used numerical models to analyse the structural properties of hybrid composites comprising carbon fibre, glass fibre, and basalt fibre under static loading conditions. Through numerical simulations, it was determined that hybrid laminates with carbon fibres positioned at the outer layers exhibit superior bending strength, as this configuration enables the carbon fibres to bear most of the transverse load, thereby improving the overall performance. Furthermore, composites incorporating basalt fibres displayed better bending strength than those containing glass fibre.

While numerous studies in the literature have focused on the use of FE models to investigate the mechanical behaviour of hybrid epoxy composites, many of these works primarily address sandwich configurations rather than double-layer configurations. The latter can offer a more integrated and reliable structure for bending applications by maximizing material performance where it counts, simplifying manufacturing processes, and reducing potential failure modes associated with core-skin interfaces in sandwich structures. Despite the known advantages of this configuration, the exact mechanisms governing the failure of such structures remain insufficiently understood. Therefore, the aim of this work is to investigate the failure mechanisms that govern bilayer hybrid composites, with a particular focus on exploring the differences in hybrid configurations and how failure evolves in these types of structures.

MATERIALS AND METHODS

In terms of materials, Sicomin provided the two-component epoxy resin SR8100 and SD8824, which were used as the matrix, while Rebelco supplied the woven bidirectional carbon fabric 195T (196 g/m^2) and the woven bidirectional glass fabric 1195P (195 g/m^2) for the reinforcements. As shown in Fig. 1, a total of eight lay-up configurations were manufactured using the following combinations: "1G/7C," "7C/1G," "2G/6C," "6C/2C," "3G/5C," "5C/3G," "8C," and "8G". In detail, after five minutes of mixing the resin and hardener using a mechanical stirrer at 300 rpm, followed by the removal of air bubbles in a vacuum chamber, the resulting system was employed to manufacture composite laminates using the hand lay-up technique. To ensure a consistent fibre volume fraction and uniform thickness, all configurations produced were placed into vacuum bags and compressed in a hydraulic press for 24 hours with a force of 2.5 kN. For the first 30 minutes, the vacuum bag was connected to a vacuum pump to eliminate all air bubbles that might have been introduced in the composite laminates during their production. Lastly, the various laminates underwent a 4-hour post-curing process at 40°C. Using the manufactured composite laminate panels, specimens of 60×10×t mm^3 were cut for the bending tests. The averaged thicknesses "t" obtained were: 1.4 mm for the “8C” configuration, 1.52 mm for “8G”, 1.50 mm for “1G/7C” and “7C/1G”, 1.49 mm for “2G/6C” and “6C/2G”, and 1.49 mm for “3G/5C” and “5C/3G”. The specimens were subjected to 3-point bending (3PB) tests following the ISO 178-2019 standard using a Shimadzu AG-X universal testing machine

equipped with a 10 kN load cell, a 35 mm span between supports, and a displacement rate of 2 mm/min. To ensure statistical reliability, a minimum of eight specimens were tested for each condition under the parameters illustrated in Fig. 2.

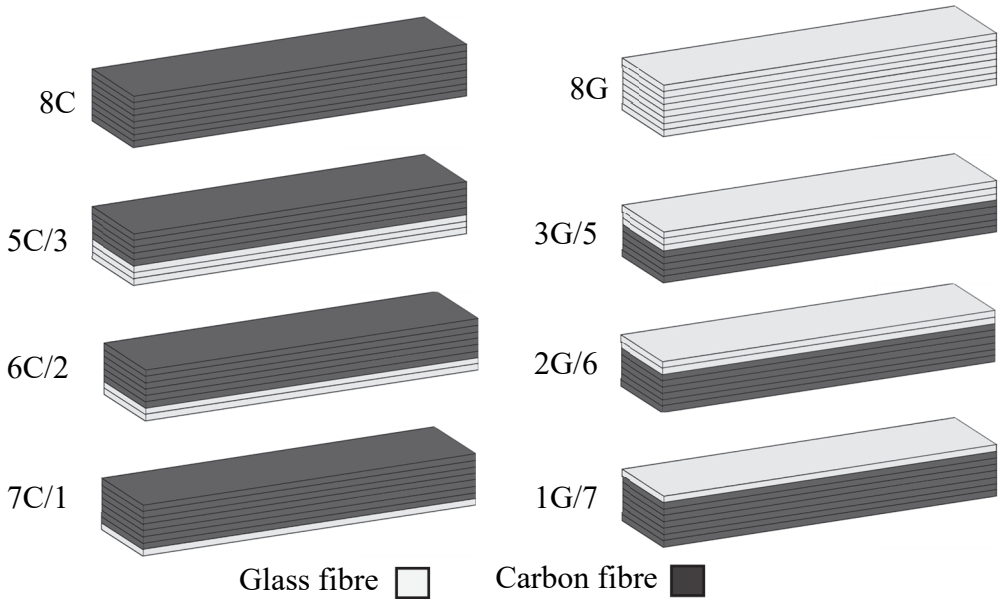

Figure 1: Lay-up configurations of all composite laminates employed.

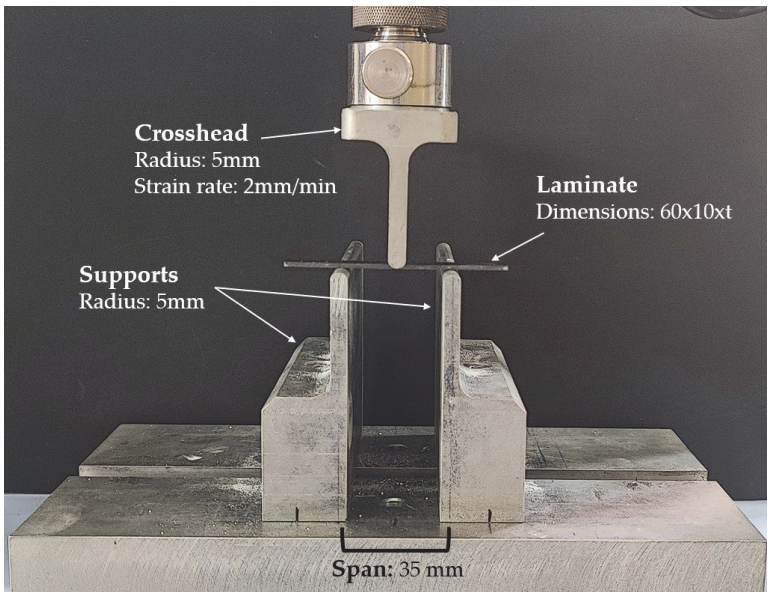

Figure 2: Experimental setup for the bending tests in accordance with ISO 178-2019.

NUMERICAL MODELS

To replicate the experimental 3PB tests described in Section 2, 3D FE models were developed in ABAQUS® FE. The laminate layers were modelled using 8-node continuum shell elements (SC8R), while the crosshead and supports were represented using 4-node discrete rigid elements (R3D4). Due to the negligible thickness of the layer interfaces, cohesive surfaces were employed to model the bonding, eliminating the need for explicit element definition. The 3D FE mesh was refined in the contact regions be-tween the specimen/crosshead and the specimen/supports, as shown in Fig. 3. This refinement ensures an accurate representation of stress concentrations and gradients near the loading points and supports, leading to more precise predictions of the bending loads.

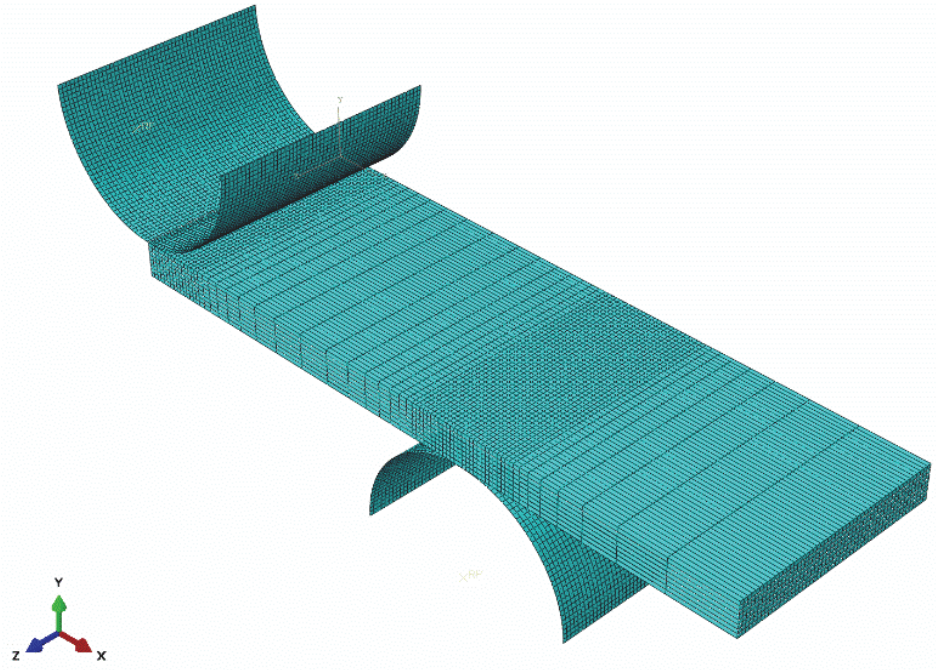

Figure 3: 3D FE model developed to analyse the different laminate configurations under 3PB loading.

To recreate the experimental setup, fixed boundary conditions were set for both supports, and a gradually increasing displacement (u_y) was applied to the crosshead. For improved computational efficiency, only half of the geometry was modelled, taking advantage of the symmetry. As a result, symmetric boundary conditions were enforced along the ZY-plane. The 3D FE model comprises of 35,464 elements and 64,660 nodes. A friction coefficient of 0.3 was assigned to the crosshead-composite and supports-composite interactions, while a coefficient of 0.5 was used for the layer interfaces [5].
To simulate the intralaminar (matrix cracking and fibre breakage) and interlaminar damage (delamination) mechanisms, two damage models were used: the continuum damage mechanics (CDM) model used for intralaminar damage and the surface-based cohesive behaviour (SbCB) model for interlaminar damage. The CDM was implemented using an ABAQUS® VUMAT subroutine for fabric-reinforced composites. This model uses the maximum stress failure criterion to identify the onset of fibre damage. The proposed approach also incorporates fracture energies to account for stiffness re-duction due to matrix cracking, plastic deformation under shear loading, and fibre failure.
Tab. 1 lists the VUMAT subroutine inputs for the carbon- and glass-fabric-reinforced composite layers used in this study. The subscripts "+" and "-" denote the tensile and compressive loading modes, respectively, while "1" and "2" refer to the principal directions of the layer. The strength ($X_{1+,-}$=$X_{2+,-}$ and S), elastic properties ($E_{1+,-}$=$E_{2+,-}$ and G_{12}), and the fracture energies (G_f^{12}), were initially estimated from the experimental data. The remaining parameters required for the constitutive model, such as the maximum shear damage (d_{12}^{max}), initial effective shear yield stress (σ_{y0}), and the coefficient (C) and power term (p) in the hardening function, were obtained from [6]. Nevertheless, it should be noted that these values were then optimised through a parametric study to ensure a satisfactory correlation with the experimental results, thereby ensuring a satisfactory representation of the laminate behaviour.

Fibers	ρ kg/m^3	$E_{1+,-}$=$E_{2+,-}$ GPa	G_{12} GPa	ν_{12}	$X_{1+,-}$=$X_{2+,-}$ MPa	S MPa	$G_f^{1,2}$ N/mm	d_{12}^{max}	σ_{y0} MPa	C	p
Carbon	1900	40	3	0.14	640	120	15000	1	55	800	0.552
Glass	1600	9.5	0.11	0.11	320	40	25000	1	25	800	0.552

Table 1: Intralaminar properties of the carbon and glass fabric-reinforced composite layers.

The interlaminar bonding between the layers was simulated using the SbCB model, which is suitable for interfaces with negligible thickness. This model utilises a traction-separation constitutive model to govern cohesive behaviour. The required parameters to define the model were based on previous studies conducted by the authors [6]. In this way, the stiffness (k_n=k_s=k_t) values used were 106 N/mm^3, the damage initiation (τ_{n0} and τ_{s0} = τ_{t0}) were 50 MPa and 42 MPa, respectively,

damage evolution energies (G_{Ic} and G_{IIc}=G_{IIIc}) were 0.5 J/m² and 2 J/m², respectively, and the interaction parameter (η) was 1.45. To ensure the accuracy and reliability of the numerical predictions of the quasi-static analysis using the ABAQUS® explicit dynamic solver, the loading velocity was limited to 1.2 m/s, and the stable time increment was maintained below 1.5×10^{-8} s throughout the analysis [7, 8]. To minimise stress wave propagation within the model, a smooth ramp-up of the loading velocity was applied.

RESULTS AND DISCUSSION

Experimental data

The experimental results are shown in Fig. 4. Since the standard deviations for the average force and displacement range from 2% to 15% and 2.5% to 12%, respectively, the typical force-displacement curves are representative of each configuration and provide strong reproducibility of the results.

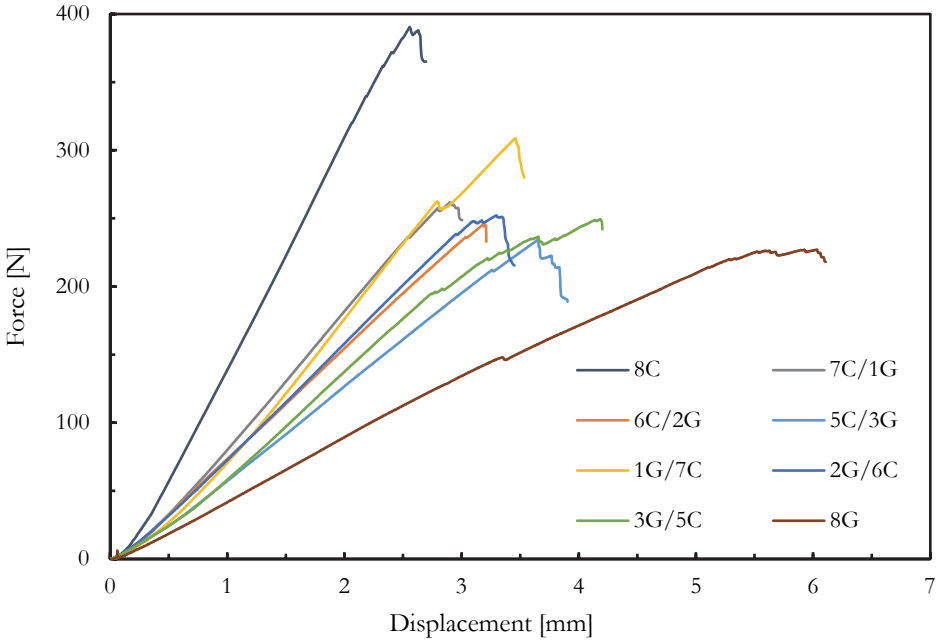

Figure 4: Force-displacement curves for laminates with: a) Glass fibres in the compressive side; b) Glass fibres in the tensile side.

The force increases with displacement in all composites almost linearly until it reaches a peak value, at which point it rapidly decreases. Furthermore, in the region of maximum force, certain curves exhibit a pronounced zigzag pattern, which is explained by the successive failure of various fibres. This is especially evident for hybrid composites that have carbon fibres on the compression side because the high stress concentration in the pin-load contact region associated with the low compressive strength of the fibres encourages their breakage and the resulting zigzag appearance [9, 10].

Hybrid laminates, which exhibit a strong dependence on the hybridisation rate, exhibit load and displacement values between those observed for nonhybrid carbon and glass laminates. For example, carbon fibre laminates exhibit the highest load (366.6 ± 27.7 N), while glass laminates exhibit the lowest with a value of 219.6 ± 5.5 N. This trend was reversed when the displacement was considered in the maximum load, with values of 2.58 ± 0.2 and 5.96 ± 0.18 mm, respectively. Further evidence for hybrid laminates is the fact that, regardless of their location, the greater number of fibreglass layers leads to a lower bending force and greater displacement. However, when these were in the compression region of the specimen, the results for force and displacement are slightly higher. This is justified by the fact that glass fibres present strains around 650% greater than carbon ones and, consequently, greater toughness [11, 12], while carbon fibres are four times stiffer and have 20–50% greater tensile strength [13, 14]. Furthermore, the latter are characterised by a compressive strength between 30% and 50% of the tensile strength, which makes them more sensitive to compression than glass fibres [15]. Based on these intrinsic properties of fibres, damage in carbon fibres occurs by breakage on the compression side and some delamination around them, whereas in glass fibres they break on the tensile side [9, 16, 17].

Numerical predictions

Figs. 5 and 6 show that all numerical values fell within the standard deviation range of the experimental results, demonstrating a good degree of correlation between the two sets of data.

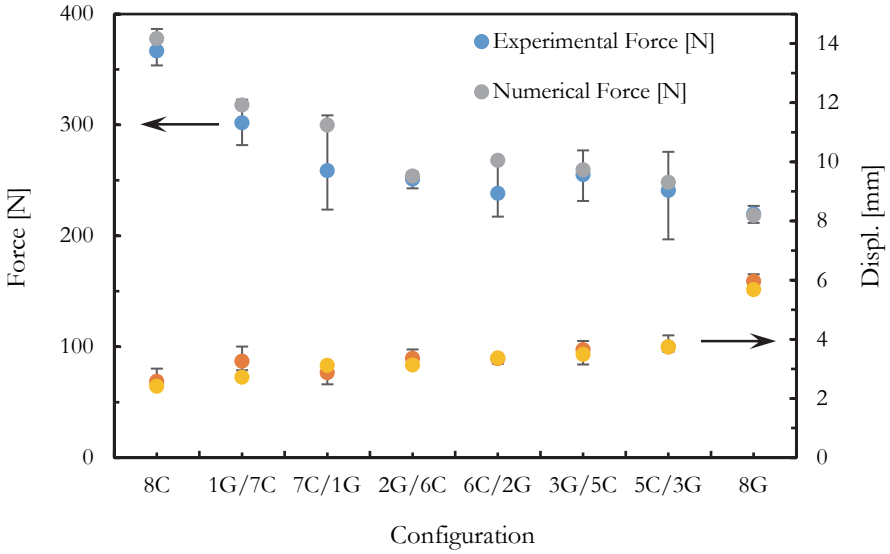

Figure 5: Comparison between experimental and numerical results for maximum force and corresponding displacement.

Particularly, as shown in Fig. 5, the numerical predictions are slightly higher than the experimental values, with errors of 3.1% for 8C, 5.3% for 1G/7C, 15.9% for 7C/1G, 11% for 6C/2G, 1.7% for 3G/5C, 1.7% for 5C/3G, and -0.5% for 8G. The results for the maximum displacement indicate that the presence of more than one layer of glass fibre on the bottom of the laminate (7C/1G, 6C/2G and 5C/3G), results in an overestimation of the numerical predictions with errors of 8.7% for 7C/1G, 0.6% for 6C/2G, and 0% for 5C/3G. On the other hand, for the remaining configurations, the maximum displacement obtained numerically was lower than that obtained experimentally. Specifically, the numerical results presented errors of -6.6% for 8C, -3.67% for 1G/7C, -6.8% for 2G/6C, -17.5% for 3G/5C, and -4.7% for 8G.

Analysing the force-displacement curves represented in Fig. 6a and 6b, it is possible to notice that numerical and experimental results have a similar behaviour throughout the 3PB test and that they present a satisfactory agreement for all tested configurations.

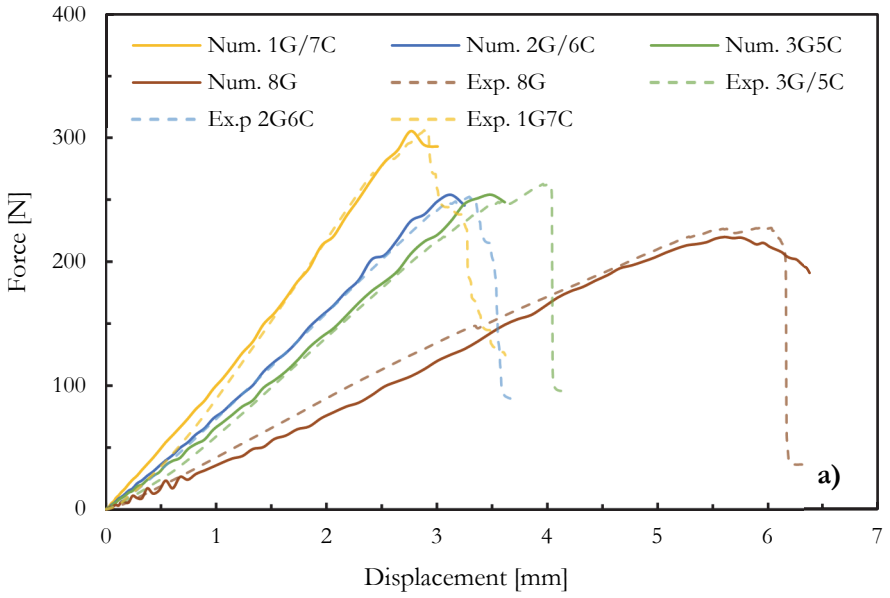

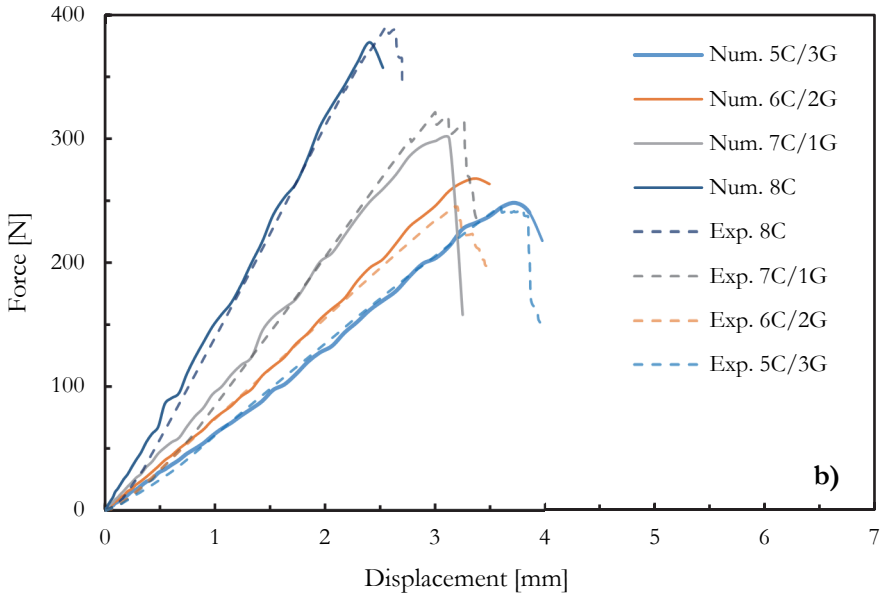

Figure 6: Comparison between experimental and numerical results for: a) 1G/7C, 2G/6C, 3G/5C, and 8G; b) 8C, 5C/3G, 6C/2G, and 7C/1G.

Since the numerical simulations were conducted using the ABAQUS®/Explicit solver to model the behaviour of the material under quasi-static loading, it is important to acknowledge that the explicit time integration scheme introduces minor dynamic effects. These effects manifest as slight oscillations or waviness that can be appreciated in the force–displacement curves. To ensure the accuracy and reliability of the results, quasi-static conditions were maintained by closely monitoring the kinetic energy, which was kept below 5% of the internal energy throughout the simulations. Additionally, mass scaling techniques were avoided.

The energy dissipation mechanisms associated with intralaminar, interlaminar damage, and frictional effects for all configurations are shown in Fig. 7a, Fig. 7b, and Fig. 7c, respectively. In each figure, the dashed vertical lines indicate the displacement corresponding to the peak force (denoted as "Max. disp.") for each laminate configuration. This helps contextualize the onset and evolution of damage mechanisms relative to the mechanical performance of the laminates. To improve the clarity and comparability of the results, the axes were rescaled appropriately, allowing for a better visual interpretation of the different energy dissipation mechanisms. Notice that the energy dissipation values were extracted directly from the ABAQUS®/Explicit output database. Specifically, the intralaminar and interlaminar damage energy dissipation values were derived from the built-in output variables ALLPD (Plastic Dissipation Energy) and ALLDMD (Damage Dissipation Energy), respectively. Additionally, the energy dissipated through frictional effects was obtained from the ALLFD (Frictional Dissipation Energy) variable.

When comparing the three types of damage, it can be concluded that intralaminar is the main damage mechanism for all configurations, followed by delamination. Moreover, as shown in Fig. 7a, the samples with glass fibre on the compressive side exhibit a reduced level of damage up to the maximum displacement point. Conversely, the samples with glass fibre on the tensile side demonstrated a higher propensity for intralaminar damage before to reaching the peak force. These observations are consistent with previously reported results [11-14]. Furthermore, a discernible change in slope is evident in the samples with the aforementioned configuration after reaching the maximum peak force, while the samples with the opposite configuration do not exhibit an increase in slope after this point. Analysing the results of the delamination in Fig. 7b it can be observed that delamination occurs only after reaching the peak force point for all samples. The 8C sample has a higher degree of delamination compared to the hybrid samples, which a have a similar behaviour among all configurations with no only a higher initial increase of delamination in the configurations with the glass in the tensile side, on the other hand, the sample containing only glass fibre presents almost no delamination, which is in line with the works available in the literature [18, 19]. Looking at the friction results in Fig. 7c two different behaviours can be observed depending on the location of the glass layers. When the glass fibres are in the compressive side, the friction increased until the end of the test.

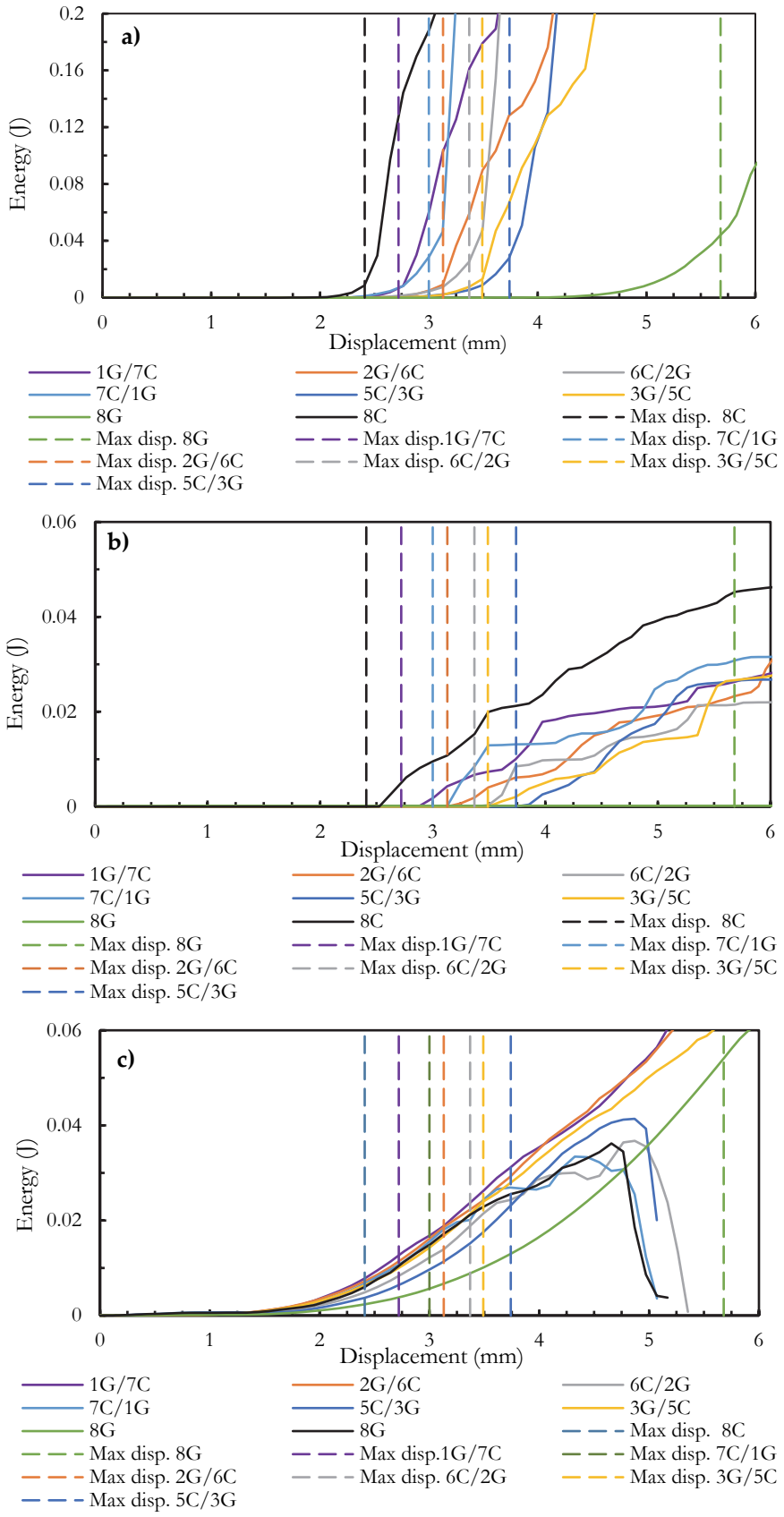

Figure 7: Energy dissipated during the 3PB test for all laminate configurations by: a) Intralaminar damage; b) Delamination; c) Friction.

On the other hand, the samples with glass fibre in the tensile side showed a sudden drop after reaching the maximum force. Beyond this point, the layers may start to separate or fail, reducing the frictional forces between them. In addition, layer separation can reduce the contact area between layers, resulting in a drop in friction energy as there is less interfacial interaction [20-22].

As noticed by the preceding results, intralaminar damage was the primary damage mechanism in the bending tests for all configurations. To further understand the intralaminar behaviour, energy dissipated by the intralaminar damage layer was analysed, as shown in Fig. 8. In the context of these results, lamina #1 is defined as the lamina closest to the loading pin, while lamina 8 is the lamina at the bottom. The data indicates that, for hybrid composites, the most external carbon fibre layer exhibited an increase in intralaminar energy. In samples with glass fibre on the compressive side, this corresponds to layer #8, whereas for samples with glass fibre on the tensile side, it corresponds to layer #1. It is noteworthy that the samples with more interior layers exhibited minimal damage, with the layer #4 exhibiting the least damage overall across all configurations. Furthermore, samples with higher numbers of glass layers demonstrated reduced intralaminar damage before maximum force compared to samples with higher amounts of carbon fibre layers. A comparison of carbon- and glass-only laminates with hybrid laminates reveals that for both configurations, the exterior layers were the first to experience damage. For the 8C laminate (Fig. 8g), the damage was first observed in layers #1 and #8, while in the 8G composite (Fig. 8h), the order was reversed, with layer #8 exhibiting the earliest damage, followed by layer #1. A closer examination of the damage evolution reveals that the 8C laminate undergoes a more pronounced and rapid increase in damage. These outcomes are analogous to those observed in hybrid composites with a greater number of carbon layers, resulting in behaviours analogous to those of 8C composites. In contrast, the 8G laminate exhibited a more gradual increase in intralaminar damage. Moreover, to understand how damage propagates throughout the hybrid laminate samples, figures were captured at various displacement points to document the progression of ten-sile, compression, and delamination damage. The outcomes for the 6C/2G hybrid sample, which serves as a representative specimen in this case, are presented in Figs. 9, 10, and 11.

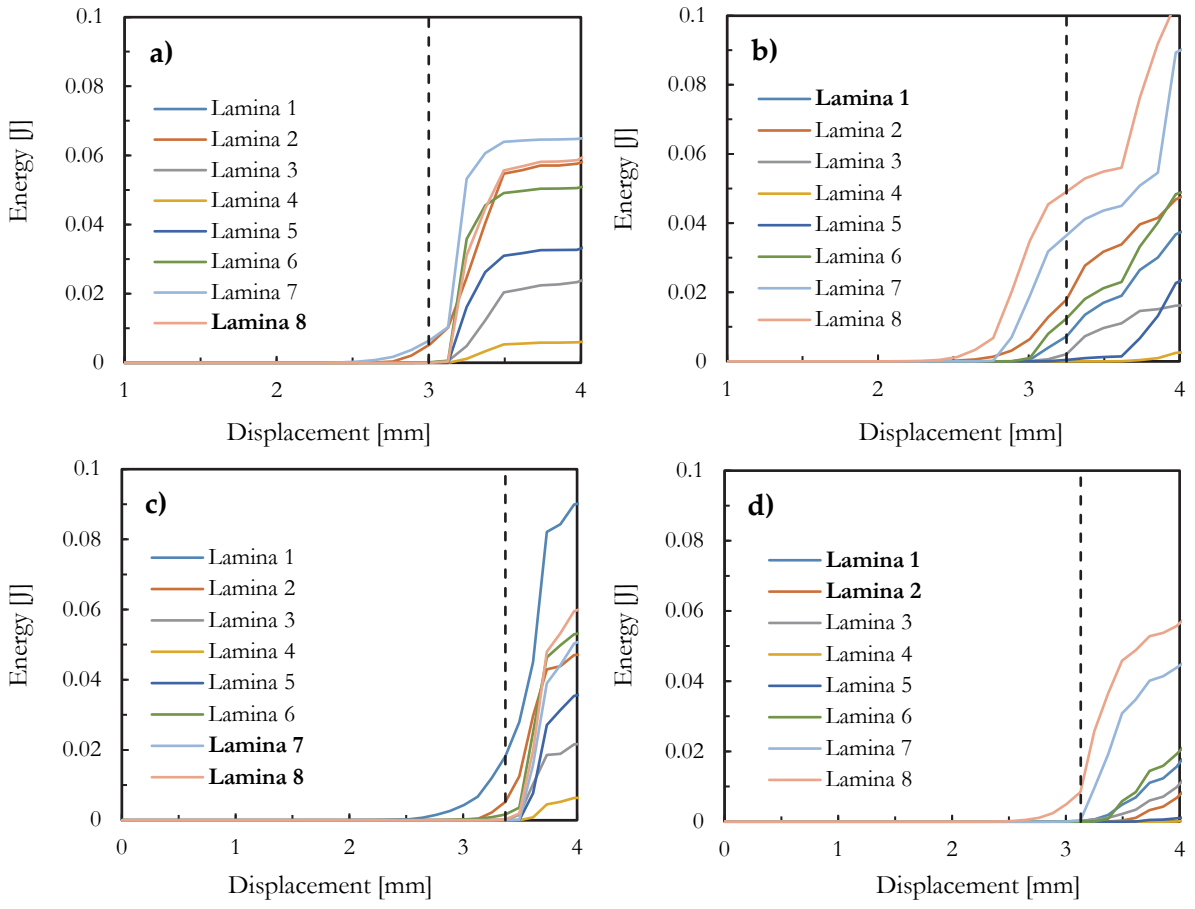

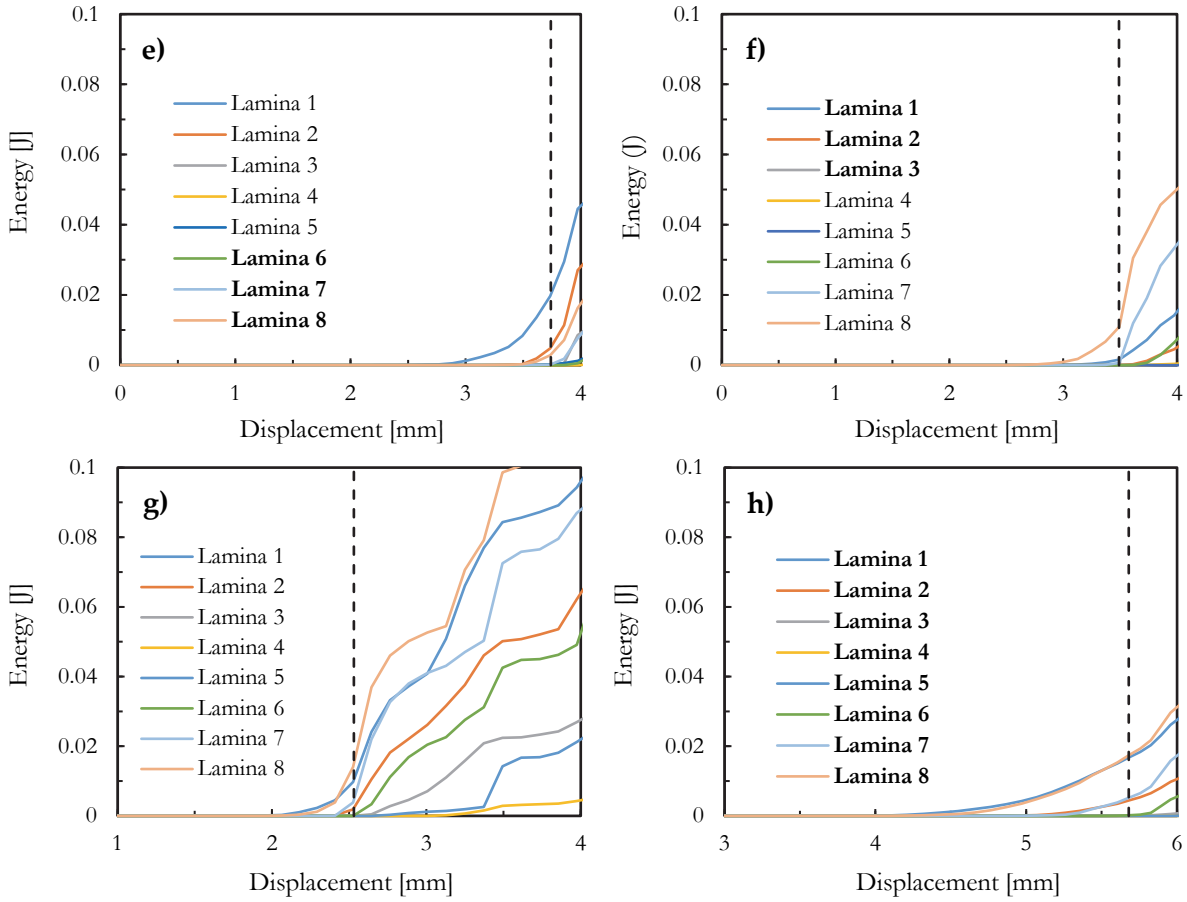

Figure 8: Energy dissipated by intralaminar damage in each layer for: a) 7C/1G; b) 1G/7C; c) 6C/2G; d) 2G/6C; e) 5C/3G; f) 3G/5C; g) 8C; h) 8G. Bold represent laminas composed by glass fibre. The dashed lines represent the displacement at the peak force.

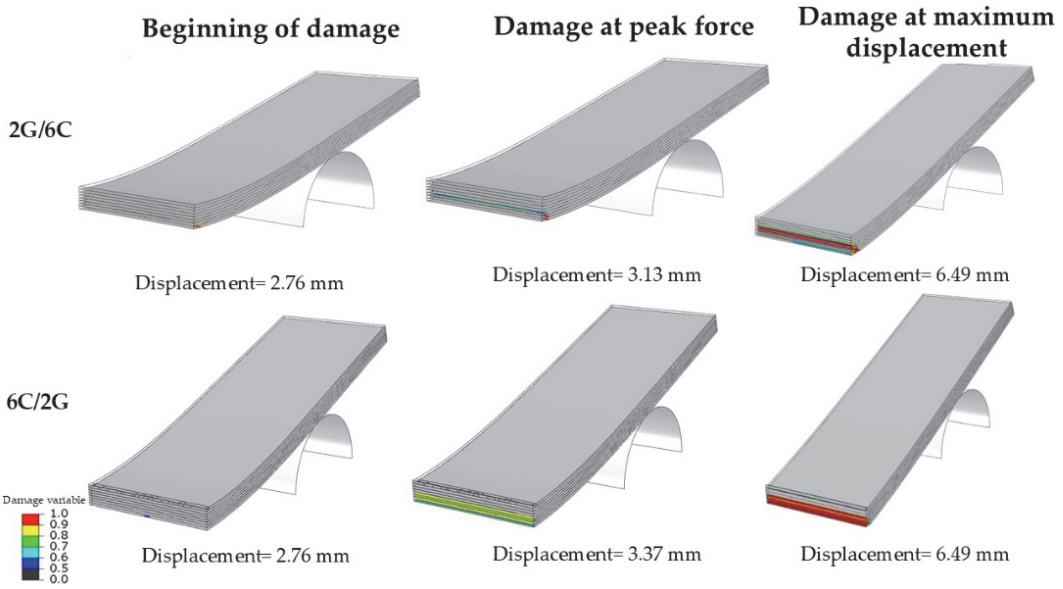

Figure 9: Tensile damage in hybrid laminate configurations 2G/6C and 6C/2G.

As depicted in Fig. 9, the tensile damage results indicate that for the 2G/6C configuration, the damage is observed in layers #7 and #8, which correspond to the final two layers of carbon fibre behind the centre of the specimen. As the sample reaches the peak force, the damage propagates up to layer #6, at which point the sample's mechanical performance begins

to deteriorate. The specimen's failure is characterised by the propagation of damage up to layer #4, accompanied by severe damage accumulation between layers #5 and #8. Upon reaching the maximum displacement, the damage does not continue to spread upwards; rather, it progresses further away from the centre of the sample. The results for the 6G/2C configuration demonstrate that the initial damage manifests in the centre of the sample in the last layer. Upon reaching the peak force, the damage propagates to the fifth layer. Beyond this point, the sample experiences complete failure accompanied by a more pronounced intensification of the damage than in the 2G/6C configuration. It is noteworthy that as the maximum displacement is attained, no further escalation in the tensile damage is observed. The disparity in behaviour exhibited by these two configurations can be attributed to the inherent properties of the carbon fibres and glass fibres used. Due to its higher stiffness, carbon fibre exhibits a greater capacity to absorb tensile damage than the glass fibre. Consequently, the progression of damage is observed to be more gradual in the 2G/6C configuration in comparison to the 6C/2G configuration, in which glass fibres are positioned along the tensile side [11, 13, 23].

The findings of the compressive damage investigation in Fig. 10 indicate that, for the 2G/6C configuration, the damage initiates in the primary glass fibre layer. Upon attaining the maximum force, there is no escalation in the number of affected layers. After this point, the compressive damage disseminates to layer #2, resulting in substantial damage in these regions. When the maximum displacement is reached, there is no further augmentation of the damage. In the 6C/2G configuration, the damage is initiated in layer #2 of the glass fibre. As the maximum force is reached, the damage disseminates to layer #3, which corresponds to the initial layer of carbon fibre. After reaching the maximum force, the damage disseminated to the lower layers of carbon fibre, extending to layer #4. The difference between 2G/6C and 6C/2G is attributed to the properties of the glass fibres. The position of the glass fibre in the compression side has a delaying effect on the formation of compression damage, which consequently forces it to initiate in the carbon fibre, which exhibits a reduced capacity to absorb this particular type of damage. This effect is in contrast with the behaviour observed in tensile damage and with previous reports [11, 24].

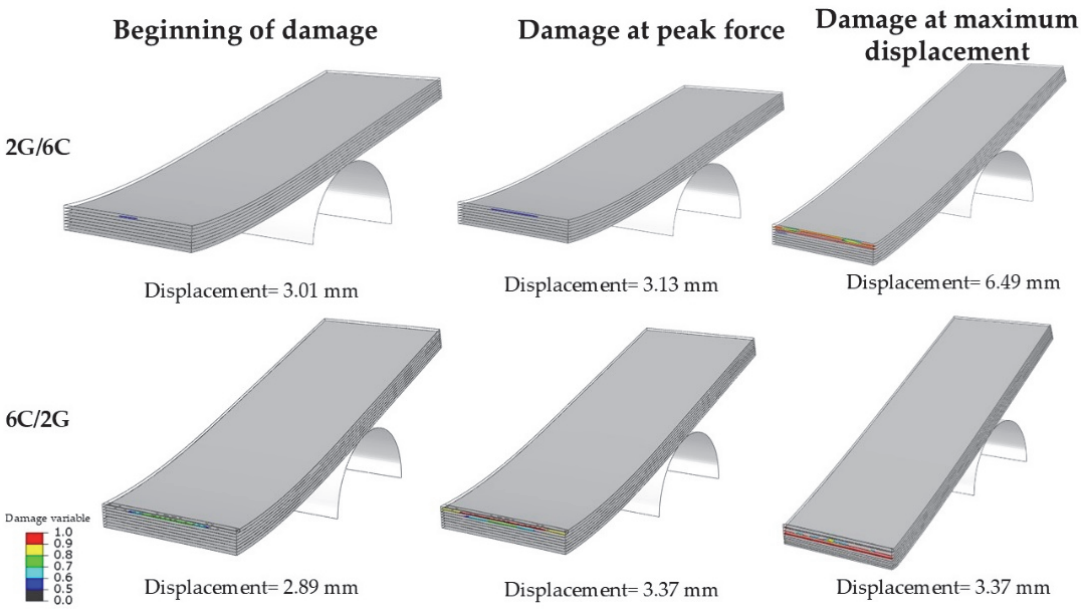

Figure 10: Compressive damage in hybrid laminate configurations 2G/6C and 6C/2G.

The delamination damage shown in Fig. 11 indicates that for the 2G/6C laminate, the delamination damage starts in the last two layers of carbon fibre.

When the maximum force is reached, the delamination spreads further away from the centre of the specimen. As the failure spreads through the laminate, the delamination damage increases upward to the other carbon fibre layers but does not spread to the glass fibre layers. For the other configuration the behaviour is similar. The initial damage manifests in the same layers. However, due to the absence of glass fibre on the compressive side to absorb the damage, the delamination became more severe and extended farther from the centre of the laminate. Upon reaching the maximum displacement, visible separation occurs between the glass and carbon fibre layers, as well as between the initial carbon fibre layers. This behaviour is similar to that previously observed and is consistent with the existing literature [12, 25].

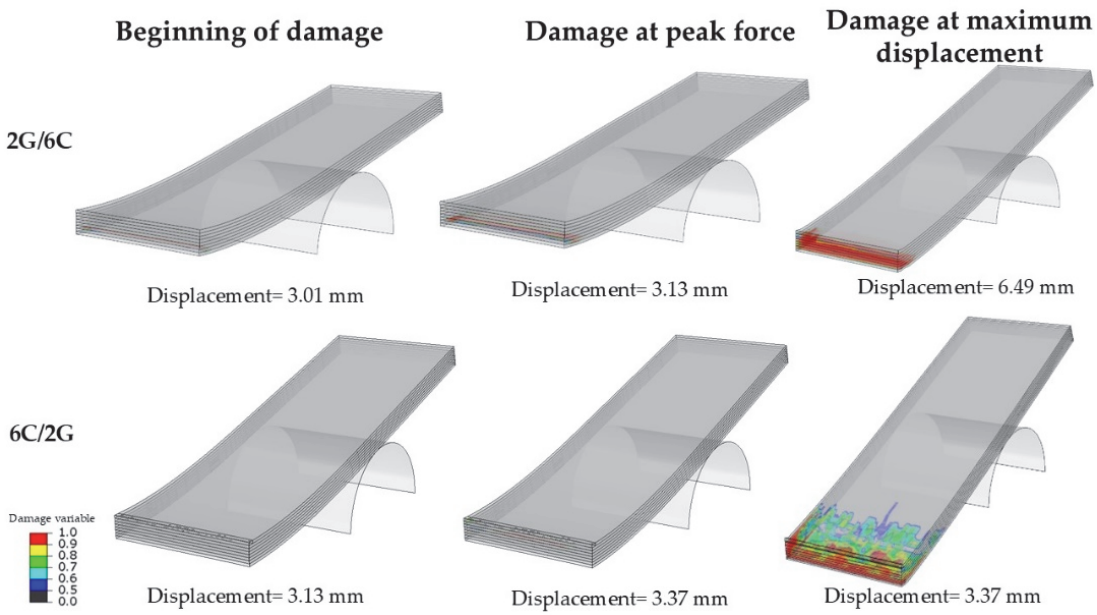

Figure 11: Delamination damage in hybrid laminate configurations 2G/6C and 6C/2G.

CONCLUSIONS

This study analysed the failure mechanisms of hybrid composites consisting of carbon and glass fibres within an epoxy matrix when subjected to bending loads. The results demonstrate the influence of hybridisation on mechanical performance, particularly in terms of strength, displacement, and damage evolution. Based on the experimental and numerical analysis conducted, the following conclusions can be drawn:

- Carbon fibre laminates achieved the highest bending strength (366.6 ± 27.7 N), while glass fibre laminates recorded the lowest (219.6 ± 5.5 N). However, this trend reversed when considering displacement at maximum load, with carbon fibre laminates showing the lowest values (2.58 ± 0.2 mm) and glass laminates the highest (5.96 ± 0.18 mm).
- The hybrid laminates exhibited mechanical properties that are between those of non-hybrid carbon and glass laminates.
- The positioning of glass fibres plays a crucial role in determining the bending strength and displacement, because when placed on the compression side of the specimen they promoted higher bending strength and lower displacement, while on the tensile side they led to lower strength but higher displacement.
- In terms of failure mechanisms, intralaminar damage emerged as the primary mode of failure across all configurations, followed by delamination. Hybrid samples where glass fibres were positioned in the compression region exhibited reduced damage up to the point of maximum displacement. In all specimens, delamination initiated at the peak force, with carbon fibre laminates displaying a greater degree of delamination than hybrid configurations. In contrast, laminates composed entirely of glass fibres exhibited minimal delamination.
- Frictional behaviour was also influenced by the fibre arrangement. When glass fibres were positioned in the compression zone, friction increased steadily until the test was concluded. Conversely, when the glass fibres were placed on the tensile side, a sudden drop in friction occurred immediately after reaching the peak load.
- Intralaminar energy dissipation was most pronounced in the outermost carbon fibre layers of the hybrid laminates.
- Composites with a higher proportion of internal layers exhibited less damage propagation, whereas increasing the number of glass fibre layers led to lower intralaminar damage before reaching the peak force, compared to configurations with more carbon fibre content. Delamination behaviour also differed between hybrid configurations. In the 2G/6C laminate, delamination first appeared in the last two carbon fibre layers and progressively spread through additional carbon layers without reaching the glass fibres. In contrast, the 6C/2G configuration exhibited a similar initial damage pattern but with more severe delamination progression.

In summary, understanding the influence of the fibre arrangement on the mechanical performance and failure evolution can contribute to the optimisation of hybrid composite designs, particularly in structural applications where bending resistance and controlled damage progression are of critical importance.

ACKNOWLEDGMENTS

This research was sponsored by national funds through FCT— Fundação para a Ciência e a Tecnologia, under projects UID/00285 – Centre for Mechanical Engineering, Materials and Processes and LA/P/0112/2020; J.M. Parente thanks FCT—Fundação para a Ciência e a Tecnologia, for the grant UI/BD/151477/2021 (https://doi.org/10.54499/UI/BD/151477/2021). This work was supported by the following projects and organisms: Portuguese Foundation for Science and Technology, I.P. (FCT, I.P.) FCT/MCTES through national funds (PIDDAC), under the R&D Unit CMAST/Center for Mechanical and Aerospace Science and Technologies, reference: Projects UIDB/00151/2020 (https://doi.org/10.54499/UIDB/00151/2020) and UIDP/00151/2020 (https://doi.org/10.54499/UIDP/00151/2020). This research was partially supported by the Spanish Ministry of Science, Innovation, and Universities, and European Regional Development Fund (PID2021-123325OB-I00). This research was partially supported by the Spanish Ministry of Science, Innovation, and Universities, and European Regional development Fund (PID2021-123325OB-I00)

REFERENCES

[1] Dong, C. (2020). Flexural properties of symmetric carbon and glass fibre reinforced hybrid composite laminates, Compos Part C-Open, 3, pp. 100047, DOI: 10.1016/j.jcomc.2020.100047.

[2] Dong, C. (2024). Flexural properties and optimisation of hybrid composites reinforced by carbon, glass and flax fibres, Hybrid Advances, 7, pp. 100302. DOI: 10.1016/j.hybadv.2024.100302.

[3] Karuppannan Gopalraj, S., Karki, T. (2021). A Finite Element Study to Investigate the Mechanical Behaviour of Unidirectional Recycled Carbon Fibre/Glass Fibre-Reinforced Epoxy Composites, Polymers (Basel), 13, pp 3192. DOI: 10.3390/polym13183192.

[4] Aslam Shaikh, A., Anil Pradhan, A., Mahesh Kotasthane, A., Patil, S., Karuppanan, S. (2022). Comparative analysis of Basalt/E-Glass/S2-Fibreglass-Carbon fiber reinforced epoxy laminates using finite element method, Materials Today: Proceedings, 63, .pp 630-638. DOI: 10.1016/j.matpr.2022.04.385.

[5] Ferreira, L.M., Muñoz-Reja, M., Reis, P.N.B. (2024). Impact response of semicylindrical woven composite shells: The effect of stacking sequence, International Journal of Impact Engineering, 189, pp. 104952. DOI: 10.1016/j.ijimpeng.2024.104952.

[6] Ferreira, L.M., C. Coelho, Reis, P.N.B. (2023). Numerical Simulations of the Low-Velocity Impact Response of Semicylindrical Woven Composite Shells, Materials, 16, pp. 3442. DOI: 10.3390/ma16093442

[7] Nozères, F., Couque, H., Boulanger, R., Quirion, Y., Bailly, P., Limido J. (2021). In Numerical modelling strategies using implicit and explicit methods to simulate quasi-static and dynamic three-points bend fracture tests of a ductile steel, EPJ Web of Conferences, EDP Sciences, 02033. DOI: 10.1051/epjconf/202125002033.

[8] Fisher, T., Almeida Jr, J.H.S., Burhan, M., Kazancı, Z. (2024). Development of a new progressive damage model for woven fabric composites, Mechanics of Advanced Materials and Structures, 31, pp. 13535-13541. DOI: 10.1080/15376494.2024.2308787.

[9] Reis, P.N.B., Ferreira, J.A.M., Antunes, F.V., Costa, J.D.M. (2007). Flexural behaviour of hybrid laminated composites, Composites Part A: Applied Science and Manufacturing, 38, pp. 1612-1620. DOI: 10.1016/j.compositesa.2006.11.010.

[10] Monjon, A., Santos, P., Valvez, S., Reis, P.N.B. (2022). Hybridization Effects on Bending and Interlaminar Shear Strength of Composite Laminates, Materials, 15, pp 1302. DOI: 10.3390/ma15041302.

[11] Ozsoy, N., Mimaroğlu, A., Ozsoy, M., Ozsoy, M.I. (2015). Comparison of Mechanical Behaviour of Carbon and Glass Fiber Reinforced Epoxy Composites, Acta Physica Polonica A, 127, pp. 1032-1034. DOI:10.12693/APhysPolA.127.1032

[12] Ochola, R.O., Marcus, K., Nurick, G.N., Franz, T. (2004). Mechanical behaviour of glass and carbon fibre reinforced composites at varying strain rates, Compos Struct, 63, pp. 455-467. DOI: 10.1016/s0263-8223(03)00194-6.

[13] Ab Ghani, A.F. (2021). Hybrid Carbon/Glass Fiber Reinforced Polymer; A Frontier Material for Aerospace Industry : A Review on Mechanical Properties Enhancement, Current Science and Technology, 1, pp. 41-51. DOI: 10.15282/cst.v1i2.6919.

[14] S. Km, P. S, S. S, N. K. (2017). Fiber Reinforced Composites - A Review, Journal of Material Science & Engineering, 06, pp. 2-6. DOI: 10.4172/2169-0022.1000341.

[15] Massarwa, E., Emami Tabrizi, I., Yildiz, M. (2021). Mechanical behavior and failure of glass/carbon fiber hybrid composites: Multiscale computational predictions validated by experiments, Compos Struct, 260, 113499.

DOI: 10.1016/j.compstruct.2020.113499.
[16] Giancaspro, J.W., Papakonstantinou, C.G., Balaguru, P.N. (2010). Flexural Response of Inorganic Hybrid Composites With E-Glass and Carbon Fibers, Journal of Engineering Materials and Technology, 132. DOI: 10.1115/1.4000670.
[17] Amaro, A.M., Reis, P.N.B., de Moura, M.F.S.F. (2011). Delamination Effect on Bending Behaviour in Carbon–Epoxy Composites, Strain, 47, pp. 203-208. DOI: 10.1111/j.1475-1305.2008.00520.x.
[18] Aymerich, F., Lecca, G., Priolo, P. (2008). Modelling of delamination growth in composite laminates by the virtual internal bond method, Composites Part A: Applied Science and Manufacturing, 39, pp. 145-153. DOI: 10.1016/j.compositesa.2007.11.012.
[19] Bruno, D., Greco, F., Lonetti, P. (2008). Interaction Between Interlaminar and Intralaminar Damage in Fiber-Reinforced Composite Laminates, International Journal for Computational Methods in Engineering Science and Mechanics, 9, pp. 358-373. DOI: 10.1080/15502280802365824.
[20] Bunsell, A.R., Harris, B. (1974). Hybrid carbon and glass fibre composites, Composites, 5, pp. 157-164. DOI: 10.1016/0010-4361(74)90107-4
[21] He, B., Wang, B., Wang, Z., Qi, S., Tian, G., Wu, D. (2020). Mechanical properties of hybrid composites reinforced by carbon fiber and high-strength and high-modulus polyimide fiber, Polymer, 204, 122830. DOI: 10.1016/j.polymer.2020.122830.
[22] Jiang, X., Gao, M., Zhu, J., Ji, H., Lang, F. (2022). Studying the Interfacial Properties of Carbon/Glass Hybrid Composites via the Nanoindentation Method, Polymers, 14, 2897. DOI: 10.3390/polym14142897.
[23] Yurii, N. (2024). Mechanical Properties of Glass Fiber and Carbon Fiber Reinforced Composites, International Journal of Advanced Research, 12, pp. 518-525. DOI: 10.21474/ijar01/19668.
[24] Wu, W., Wang, Q., Li, W. (2018). Comparison of Tensile and Compressive Properties of Carbon/Glass Interlayer and Intralayer Hybrid Composites, Materials, 11, pp 1105. DOI: 10.3390/ma11071105.
[25] Kretsis, G. (1987). A review of the tensile, compressive, flexural and shear properties of hybrid fibre-reinforced plastics, Composites, 18, pp. 13-23. DOI: 10.1016/0010-4361(87)90003-6.